AMERICAN SOCIETY FOR MICROBIOLOGY | Journal of Virology®

GENOME REPLICATION AND REGULATION OF VIRAL GENE EXPRESSION

The DNA Damage Sensor MRE11 Regulates Efficient Replication of the Autonomous Parvovirus Minute Virus of Mice

Lauren E. Bunke,[a] Clairine I. S. Larsen,[a,b] Jessica N. Pita-Aquino,[a,b] Isabella K. Jones,[a] Kinjal Majumder[a,c,d,e]

[a]Institute for Molecular Virology, Madison, Wisconsin, USA
[b]Cell and Molecular Biology Graduate Program, Madison, Wisconsin, USA
[c]McArdle Laboratory for Cancer Research, Madison, Wisconsin, USA
[d]University of Wisconsin School of Medicine and Public Health, Madison, Wisconsin, USA
[e]University of Wisconsin Carbone Cancer Center, Madison, Wisconsin, USA

Lauren E. Bunke and Clairine I. S. Larsen contributed equally to this work. Author order was determined alphabetically by last name.

ABSTRACT Parvoviruses are single-stranded DNA viruses that utilize host proteins to vigorously replicate in the nuclei of host cells, leading to cell cycle arrest. The autonomous parvovirus, minute virus of mice (MVM), forms viral replication centers in the nucleus which are adjacent to cellular DNA damage response (DDR) sites, many of which are fragile genomic regions prone to undergoing DDR during the S phase. Since the cellular DDR machinery has evolved to transcriptionally suppress the host epigenome to maintain genomic fidelity, the successful expression and replication of MVM genomes at these cellular sites suggest that MVM interacts with DDR machinery distinctly. Here, we show that efficient replication of MVM requires binding of the host DNA repair protein MRE11 in a manner that is independent of the MRE11-RAD50-NBS1 (MRN) complex. MRE11 binds to the replicating MVM genome at the P4 promoter, remaining distinct from RAD50 and NBS1, which associate with cellular DNA break sites to generate DDR signals in the host genome. Ectopic expression of wild-type MRE11 in CRISPR knockout cells rescues virus replication, revealing a dependence on MRE11 for efficient MVM replication. Our findings suggest a new model utilized by autonomous parvoviruses to usurp local DDR proteins that are crucial for viral pathogenesis and distinct from those of dependoparvoviruses, like adeno-associated virus (AAV), which require a coinfected helper virus to inactivate the local host DDR.

IMPORTANCE The cellular DNA damage response (DDR) machinery protects the host genome from the deleterious consequences of DNA breaks and recognizes invading viral pathogens. DNA viruses that replicate in the nucleus have evolved distinct strategies to evade or usurp these DDR proteins. We have discovered that the autonomous parvovirus, MVM, which is used to target cancer cells as an oncolytic agent, depends on the initial DDR sensor protein MRE11 to express and replicate efficiently in host cells. Our studies reveal that the host DDR interacts with replicating MVM molecules in ways that are distinct from viral genomes being recognized as simple broken DNA molecules. These findings suggest that autonomous parvoviruses have evolved distinct mechanisms to usurp DDR proteins, which can be used to design potent DDR-dependent oncolytic agents.

KEYWORDS parvovirus, DNA damage response, minute virus of mice, DNA damage

Cells initiate DNA damage response (DDR) signaling cascades in response to genotoxic stress to maintain the fidelity of their genomic DNA. This multistep signaling process is initiated by the recognition of broken DNA ends by MRE11-RAD50 heterodimers, which then recruit NBS1 to form the MRE11-RAD50-NBS1 (MRN) complex (1). The MRN complex

Editor Colin R. Parrish, Cornell University Baker Institute for Animal Health

Address correspondence to Kinjal Majumder, kmajumder@wisc.edu.

The authors declare no conflict of interest.

Received 27 March 2023
Accepted 7 April 2023
Published 26 April 2023

recruits and triggers autophosphorylation by the host ataxia telangiectasia-mutated (ATM) kinase at the cellular DDR site, phosphorylating local histone H2AX at serine 139 to form γH2AX platforms encompassing megabases of chromatin flanking the DNA break site (2–4). γH2AX transcriptionally represses the local chromatin to prevent aberrations caused by attempting to express damaged DNA templates (5–7). It has become increasingly clear that viral pathogens also provoke local cellular DDRs, recruiting cellular DDR pathway components to their genomes and proteins (8). However, the small size of the virus genomes, combined with efficient transcription from viral DNA templates during infection, precludes the possibility of γH2AX efficiently repressing the viral genome. This raises the question of what functions DDR proteins perform in viral genomes and how they regulate viral life cycle.

Viral and cellular genomes provoke distinct DDR signals, which have global and local effects on the nuclear environment (9). These DDR signals in the host cells are induced by viral proteins directly or in response to large amounts of viral nucleic acids that interfere with host nuclear physiology. Therefore, the cellular DDR is a barrier that must be navigated to promote successful viral infection. In the case of adenoviruses (Ad), early viral proteins target MRE11 for degradation or mislocalization (10, 11). On the other hand, in small DNA tumor viruses, polyomaviruses, and simian virus 40 (SV40), the large T antigen interacts with components of the MRN complex proteins to facilitate virus replication (12–14). By differentially interacting with cellular DDR sensors, DNA viruses have clearly evolved distinct strategies to evade or usurp the repressive effect of the cellular DDR. Despite the local transcriptionally repressive signals that surround cellular DDR sites, autonomous parvoviruses like minute virus of mice (MVM) localize to both preexisting and induced cellular DDRs (15, 16). The cellular DDR region associated with MVM replication depends on the ATM kinase, inactivates ATM kinase-related (ATR) kinase, and induces a potent premitotic cell cycle block at the G_2/M border, during which the virus replicates vigorously (17–21).

MVM is an autonomously replicating parvovirus that is lytic in mouse cells and transformed human cells (22). The viral genome is 5 kb, containing inverted terminal repeats (ITRs) at either end, which serve as origins of replication (23, 24). MVM replication is passively dependent on host cell cycle entry, using host DNA polymerases and cofactors to replicate (22). MVM encodes two viral proteins, NS1, which performs essential functions required for virus replication, and NS2, which plays important but currently undefined functions in murine hosts (25–27). Virus replication is initiated in subnuclear foci containing NS1 and NS2, viral genome, and host proteins, forming distinct viral replication centers referred to as autonomous parvovirus-associated replication (APAR) bodies (28–30). MVM-APAR bodies colocalize with sites of cellular replication, DDR, and transcription proteins, which include the sensors MRN and the DDR-associated chromatin mark γH2AX (17, 28). Despite localizing to cellular DDR sites, the MVM genome is not marked by γH2AX marks or the adapter protein MDC1, which would be detrimental to viral life cycle (15–17, 31). These findings raise the possibility that cellular DDR proteins are differentially recruited to viral genomes than to cellular DDR sites.

A possible reason for the differential recruitment of cellular DDR proteins to viral genomes is the rapid formation of single- and double-stranded DNA intermediates, especially during parvovirus replication. These replicative intermediates in the nuclear milieu have been postulated to activate local DDR signals (32, 33). In support of this model, the MRN complex associates with the related dependovirus adeno-associated virus (AAV) and recombinant AAV (rAAV) vectors at the viral ITR elements, likely contributing to transcriptional repression of the AAV/rAAV genomes by inhibiting second-strand synthesis (34, 35). Therefore, AAV replication requires coinfecting helper virus, adenovirus or herpes simplex virus (HSV), both of which have potent effects on the cellular DDR, to reverse the antagonistic effect of the local DDR and derepress the AAV genome (34, 36, 37). However, the mechanism of how DDR proteins regulate parvovirus replication cannot be discerned in the AAV system due to the impact of these essential helper viruses on the host (8). MVM, on the other hand, by virtue of its passive

and autonomous dependence on host function for virus replication, is a more permissive system to dissect how cellular DDR proteins regulate parvovirus replication.

MVM localizes to preexisting and induced cellular DDR sites and early-replicating fragile sites to establish APAR bodies in an NS1-dependent manner (15, 16). These genomic sites are enriched in DNA polymerase alpha and delta, which support MVM replication (38). Vigorous replication of MVM in the S and G_2 phases of the cell cycle generates single-stranded and double-stranded viral genome intermediates (33, 39). These genomic replication intermediates are likely to induce additional local cellular DDR signals by recruiting DDR proteins to the viral genome, which could be detrimental to viral pathogenesis. In line with these expectations, MVM replication at late G_2 (more than 30 h postinfection [hpi]) leads to proteasomal degradation of MRE11, likely precluding the induction of cellular DDR signals in the viral genomes (17). However, the role of the host cell's DDR proteins in regulating the initiation of MVM replication and formation of APAR bodies remains unknown.

Here, we have discovered that components of the MRN complex differentially associate with the MVM-APAR bodies, marking cellular sites where MVM persists as well as the viral genome. Strikingly, MRE11 associates with the replicating MVM genome at the P4 and P38 promoters in an MRN complex-independent manner. In the absence of cellular MRE11 (generated by RNA interference [RNAi]-mediated knockdown or CRISPR knockout), MVM replication is attenuated, leading to smaller APAR bodies. However, MVM replication continues in MRE11-deficient cells, suggesting the existence of redundant host pathways utilized by the virus to replicate. Overexpression of ectopic MRE11 in MRE11-deficient cells is sufficient to rescue MVM replication and APAR body formation in an MRN-independent manner. Our findings reveal that a portion of the nuclear pool of MRE11 associates with replicating MVM without forming γH2AX, while the remaining levels of MRE11 are likely involved in DDR transduction in the host genome. Furthermore, MRE11 bound to the MVM genome does not require RAD50 or NBS1 to facilitate virus replication, likely precluding the direct involvement of the MRN complex in processing the replicating MVM genome. These findings reveal new mechanisms by which DDR sensor proteins, like MRE11, regulate virus replication.

RESULTS

Distinct subsets of host MRN proteins associate with MVM-APAR bodies. MVM replicates in subnuclear viral replication centers, termed APAR bodies, which contain not only the viral genome and nonstructural proteins NS1 and NS2 but also colocalize with host RNA polymerase II, replication proteins, and DDR effectors (16, 17, 28, 29, 31). We have previously observed that, under high resolution, the DNA break-associated chromatin mark γH2AX forms foci that surround MVM-APAR bodies, suggesting MVM localizes to cellular sites of DNA damage where replication and DDR factors reside to initiate and amplify its lytic infection (16). Since γH2AX signals are transduced by the ATM kinase downstream of DNA break recognition by the MRN complex (40) and γH2AX is not detectable in the replicating MVM genome in viral nucleoprotein extracts by chromatin immunoprecipitation followed by quantitative PCR (ChIP-qPCR) (41), this raised the possibility that canonical DDR signals are not initiated in the MVM genome. To investigate the DDR proteins associated with MVM-APAR bodies, we performed high-resolution confocal imaging of nuclei from MVM-infected parasynchronous A9 cells at 16 hpi, costaining them for NS1 (red) and components of the MRN complex (green), which initiates the DDR signaling cascade. Although components of the MRN complex associated closely with MVM-APAR bodies (monitored by staining for NS1 [red]), they did not colocalize with these viral replication centers (Fig. 1A). Quantification of the median distance from NS1 foci to MRE11 foci in MVM-infected nuclei showed a median distance of 0.06 μm, which was distinct from 0.16 μm for NS1-RAD50 and 0.1 μm for NS1-NBS1 (Fig. 1B). We reasoned that the separation of staining between NS1 and MRN complex proteins may be due to differences in recruitment to the MVM genome and the adjacent cellular DDR sites. To dissect the association of the MRN complex proteins with host chromatin from that

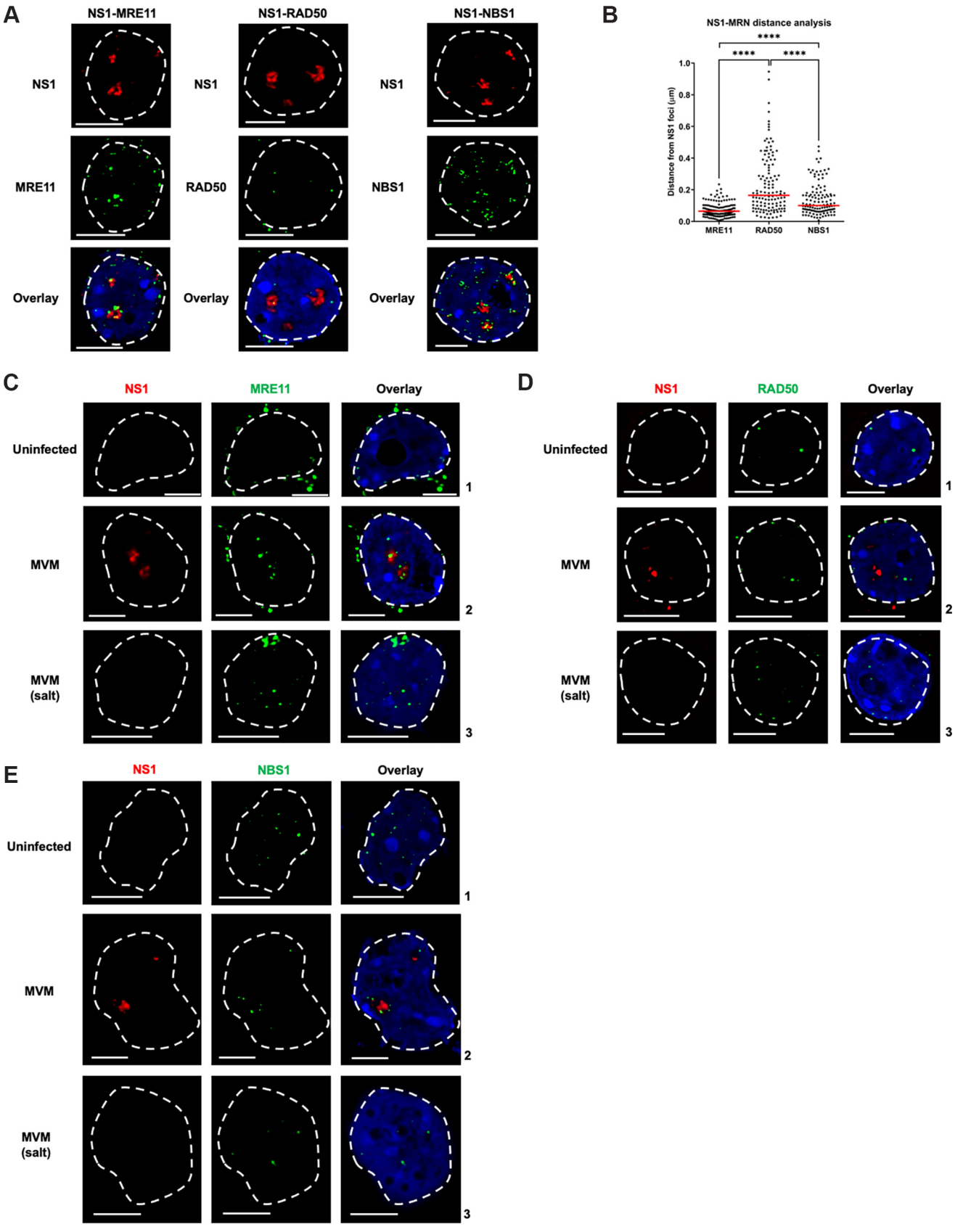

FIG 1 Distinct subsets of host MRN proteins associate with MVM-APAR bodies. (A) WT A9 cells were synchronized in isoleucine-deficient medium and then released and infected with MVM for 24 h (MOI of 10). Cells were fixed and stained for NS1 (red) and either MRE11, RAD50, or NBS1 (green) and

(Continued on next page)

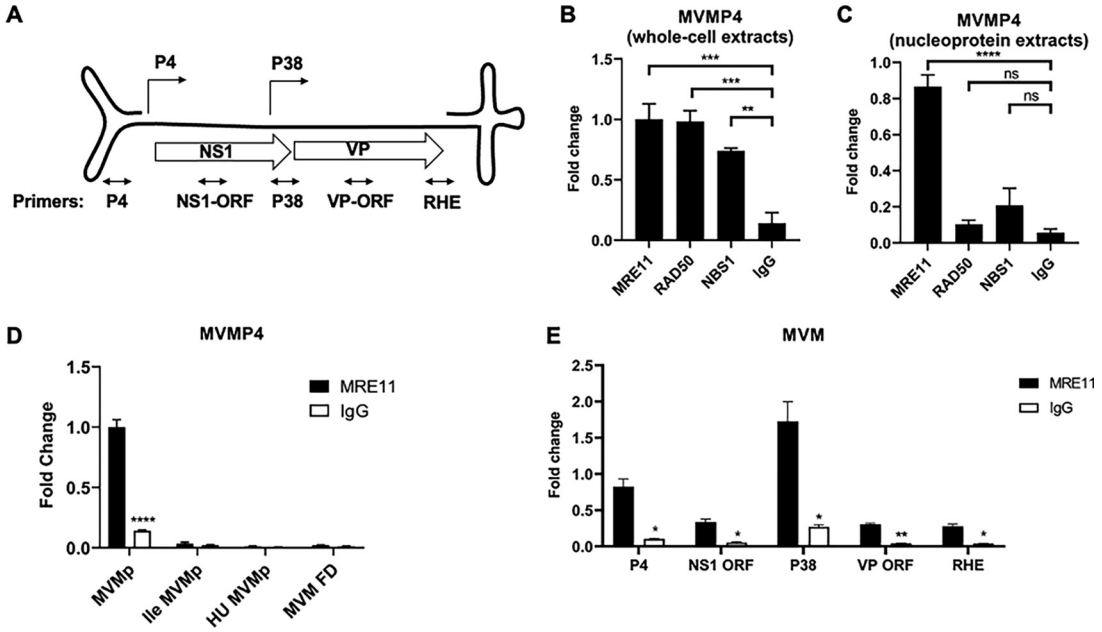

FIG 2 MRE11 binds to the replicating MVM genome independently of the MRN complex. (A) Schematic of the MVM genome with the major regulatory elements indicated on top (not drawn to scale) and labeled with the relative location of qPCR primers on the bottom (indicated by double-headed arrows). (B and C) ChIP-qPCR data for MRE11, RAD50, and NBS1 occupancy in the MVM genome at the P4 promoter when viral nucleoprotein extracts are extracted with 150 mM salt (B) and completely cross-linked with formaldehyde prior to pulldown (C). Background levels of signals were determined using total IgG as a ChIP antibody. Significant differences relative to IgG pulldown are denoted as follows: *, $P < 0.05$; **, $P < 0.005$; ***, $P < 0.0005$; ****, $P < 0.00005$; and ns, not significant (one-way analysis of variance [ANOVA], multiple-comparison test). (D) The association of MRE11 with the replicating MVM genome was determined using ChIP-qPCR at MVMP4 in MVM-infected cells, which were not allowed to enter the S phase (by continuing to block them in isoleucine-deficient media), pulsed with 2 mM hydroxyurea to induce cellular DNA damage, or transfected with 1 μg of MVM-expressing plasmid (labeled at MVM FD). The treatment conditions modulating MVM replication are designated along the *x* axis of the figure. (E) MRE11 occupancy in the MVM genome was determined on salt-extracted nucleoprotein complexes after 60 cycles of sonication by ChIP-qPCR using primers complementary to MVM sites indicated in panel A. IgG pulldown was used as negative control. Data are presented as mean ± SEM of fold change values from at least three independent experiments, where statistical significance between MRE11 and IgG pulldown are denoted as follows: *, $P < 0.05$; and ***, $P < 0.001$ (unpaired *t* test).

with the viral genome, we preextracted MVM-infected A9 cells with 150 mM salt before fixation and immunofluorescence analysis. Extraction in 150 mM salt led to the complete loss of NS1 staining and partial loss of MRE11, but no significant loss of RAD50 or NBS1 (compare rows 2 and 3 in Fig. 1C to E), suggesting a differential interaction of DDR sensor proteins with the MVM genome relative to the associated host DDR sites. Taken together, these findings suggested that the components of the MRN complex might interact with MVM-APAR bodies in distinct ways from those of canonical DDR sites.

MRE11 binds to the replicating MVM genome independently of the MRN complex. Initiation of MVM replication requires E2F-dependent activation of the MVMP4 promoter in the early S phase (42). E2F proteins additionally associate with the MRN complex at sites of DNA synthesis in the vicinity of Ebstein-Barr virus (EBV) replication origins (43). To determine whether the MRN complex proteins are associated with the MVM genome, we performed ChIP-qPCR for all three components of the MRN complex. qPCR analysis using primers complementary to the MVMP4 promoter (in DNA fragments encompassing the replication origin-containing left-hand end [LHE]) (Fig. 2A) revealed that all 3 subunits of the MRN complex are associated with the MVM genome

FIG 1 Legend (Continued)
then imaged using confocal microscopy. (B) The distance between NS1 foci and MRE11, RAD50, and NBS1 foci was measured in micrometers and is represented by a scatterplot, with red lines indicating the medians of the measurements. Statistical significance was determined as follows: ****, $P < 0.0001$ (unpaired *t* test). (C to E) WT A9 cells were synchronized and then released and infected with MVM for 16 h (MOI of 10). Cells were preextracted with a 150-mM NaCl salt solution for 5 min prior to fixation then washed with PBS and costained for NS1 (red) and either MRE11 (C), RAD50 (D), or NBS1 (E) (all green), and then imaged using confocal microscopy.

under fully cross-linked conditions (Fig. 2B). However, since MVM localizes to cellular sites of DNA damage to establish and amplify its infection (16), these findings raised the possibility of secondary cross-linking between MRN complex proteins at cellular DDR sites and the MVM genome in their vicinity. To determine whether the MRN complex proteins directly bound to the MVM genome, we performed ChIP assays on the MVM nucleoprotein extracts (previously developed by us [41]) and assayed them by qPCR on the MVM genome using primers complementary to the P4 promoter. As shown in Fig. 2C, these ChIP-qPCR assays revealed a significant binding of MRE11 to the MVM genome. Strikingly, however, neither of the other components of the MRN complex, NBS1 or RAD50, associated with the MVM genome using this modified ChIP assay, even though they were positive for the association with MVM when assessed by whole-cell cross-linking (Fig. 2C). MRE11 ChIP assays on the viral nucleoprotein extracts further revealed that MRE11 binds to the MVM genome only during viral replication, as MRE11-MVM interaction is not detected in cells that are blocked in G_0/G_1 by isoleucine deprivation or treated with hydroxyurea (Fig. 2D). Additionally, the absence of MRE11 in the MVM expression plasmid (Fig. 2D; labeled as MVM FD) suggested that viral genome expression alone is not sufficient to recruit MRE11.

To determine where MRE11 binds in the MVM genome, we combined MVM-nucleoprotein complex isolation with sonication on a Diagenode Bioruptor (detailed in Materials and Methods). Using this modified ChIP-qPCR on MVM-infected nucleoprotein extracts, we mapped the localization of MRE11 molecules in the replicating MVM genome at 16 hpi in parasynchronized A9 cells to the P4 and P38 promoters (Fig. 2E). Taken together, our findings suggested that MRE11 performs an MRN-independent role at the MVM promoters during virus replication. The absence of the complete MRN complex in the replicating and expressing viral genome is also consistent with the lack of the downstream DDR effector mark γH2AX in the MVM genome (41), which would transcriptionally repress the viral genome.

MRE11 knockdown attenuates MVM expression and replication. MRE11-mediated induction of local DDR in the viral genome is proposed to facilitate the transcriptional suppression of AAV2 and rAAV genomes (35, 37). In these instances, the coinfecting virus, such as adenovirus (10, 34, 37) or herpesvirus (36, 44), is required to derepress the local DDR by degrading or mislocalizing components of the MRN complex, facilitating expression and replication of AAV2 (8). However, autonomous viruses such as MVM replicate vigorously in the host cell's nucleus without the help of a coinfecting virus, even though MRE11 is associated with the viral genome (described above). To determine how MRE11 regulates MVM replication, we targeted the MRE11 protein using RNAi knockdown during synchronous MVM infection of A9 cells using the timeline described in Fig. 3A. Small interfering RNAs (siRNAs) targeting the *Mre11a* transcript for degradation were transfected into A9 cells during parasynchronization in isoleucine-deficient media. RNAi led to substantial depletion of MRE11 proteins at 16 hpi and 24 hpi. Cells were infected with MVMp at a multiplicity of infection (MOI) of 10 upon release, initiating S phase entry (and concurrent MVM replication) at 10 hpi. MVM replication was substantially decreased in siMre11a-transfected cells compared with siMock-transfected cells at both 16 hpi and 24 hpi (Fig. 3B; representative immunoblot on top and quantification of independent replicates on the bottom). We extended these findings to NIH 3T3 cells that were transfected with an independent siRNA (see Fig. S1A in the supplemental material), as well as human U2OS (Fig. S1B) and 324K cells (Fig. S1C) transfected with siRNAs targeting human Mre11a transcripts. In all cases, we observed a decrease in NS1 levels upon depletion of cellular MRE11. Consistent with these findings, we observed smaller APAR bodies in MVM-infected A9 cells depleted of MRE11 at 16 hpi (Fig. 3C), extending our observations to the single-cell level. Categorization of MVM-APAR bodies in at least 50 nuclei based on a previously established scheme (31) revealed that in the absence of MRE11, MVM forms mostly type 1 and type 2 APAR bodies (Fig. 3D), which are morphologically smaller than type 3, which are larger and observed mostly in the presence of MRE11 at the same time point

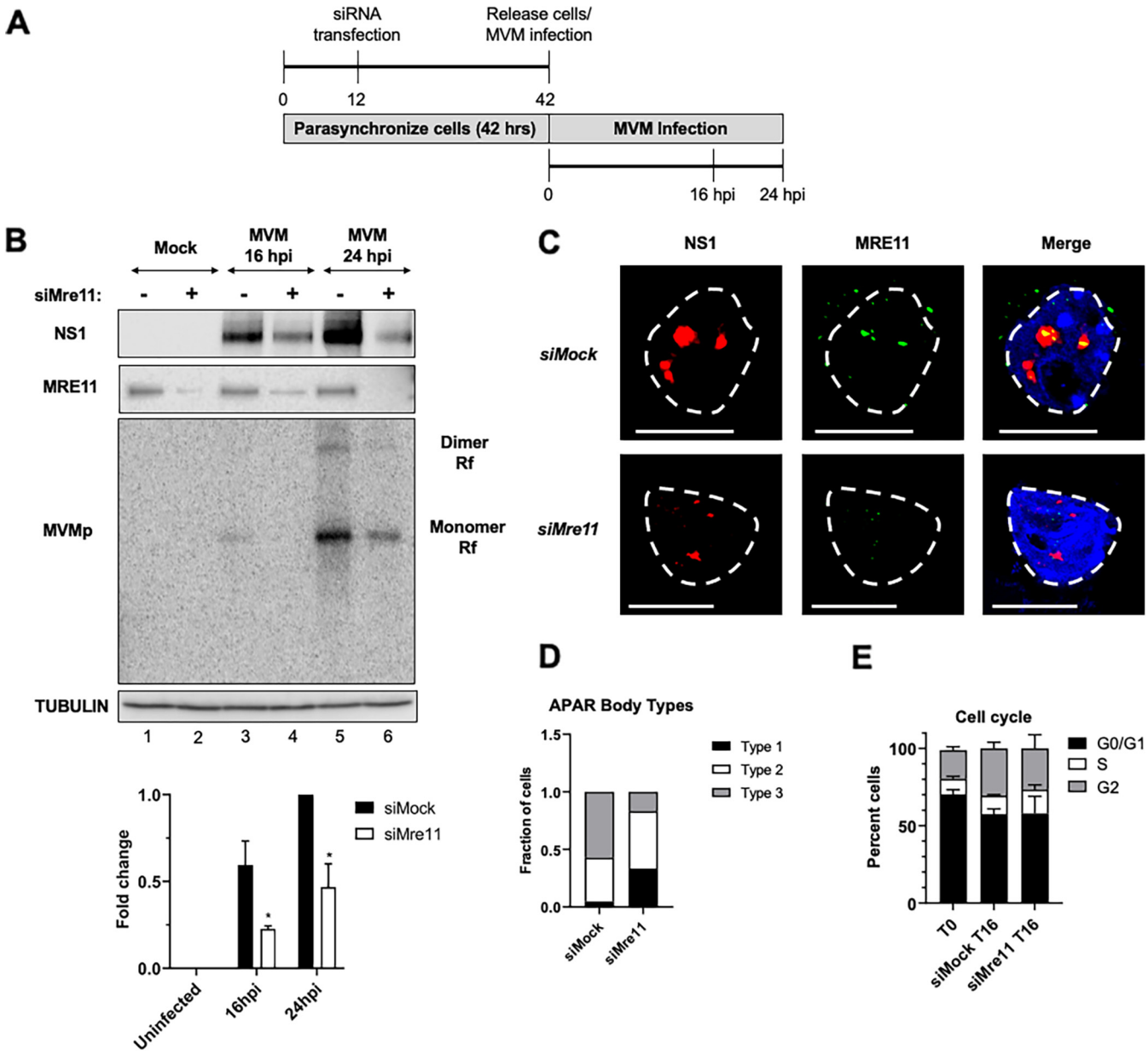

FIG 3 MRE11 knockdown attenuates MVM expression and replication. (A) Schematic illustrating the experimental procedure for RNAi-mediated knockdown of MRE11 in panels B to F. (B) Murine A9 cells were targeted with control siRNA or siRNA to *Mre11* as depicted in panel A. Uninfected control samples were harvested at 16 hpi (T16; mock). Cells were infected at the time of release at an MOI of 10 before harvest at 16 hpi and 24 hpi. Western blotting was performed using antibodies against the indicated proteins. Southern blots were performed with an MVMp genomic probe. The bottom panel quantifies the NS1 band intensity from at least 3 independent biological replicates. Statistical significance between siMock and siMre11-treated samples is denoted as follows: *, $P < 0.05$ (unpaired *t* test). (C) Murine A9 cells transfected with siMock and siMre11 were infected with MVM at an MOI of 10 for 16 h before being preextracted with cytoskeletal buffer and processed for immunofluorescence (IF) using antibodies to NS1 and MRE11. The blue signal indicates DAPI staining, nuclear borders are demarcated by broken white lines, and scale bar measures 5 μm. (D) The APAR bodies in MVM-infected A9 cells in siMock- and siMre11-transfected cells were counted in more than 100 nuclei in 3 independent experiments. APAR body characteristic was categorized as previously described (31) and presented as a fraction of total cells containing a distinct type of APAR body. (E) Murine A9 cells were synchronized as indicated above and were transfected with siMock or siMre11 during synchronization. siRNA-transfected cells at 16 hpi (indicated with T16) were processed for cell cycle analysis by propidium iodide staining followed by flow cytometry. Mock T0 cells were processed at the time of release from parasynchronization, showing the majority of cells were at a G_0/G_1 cell cycle block. Data represent the mean ± SEM of the percentage of total live cells in the gates for G_0/G_1, S, and G_2 phases of the cell cycle.

postinfection. Importantly, flow cytometric analysis of total DNA content in the presence and absence of MRE11 confirmed that host cells entered the S phase normally following this knockdown protocol and therefore did not affect the S phase-dependent initiation of MVM replication (Fig. 3E). Taken together, these findings suggested that efficient MVM expression and replication require MRE11.

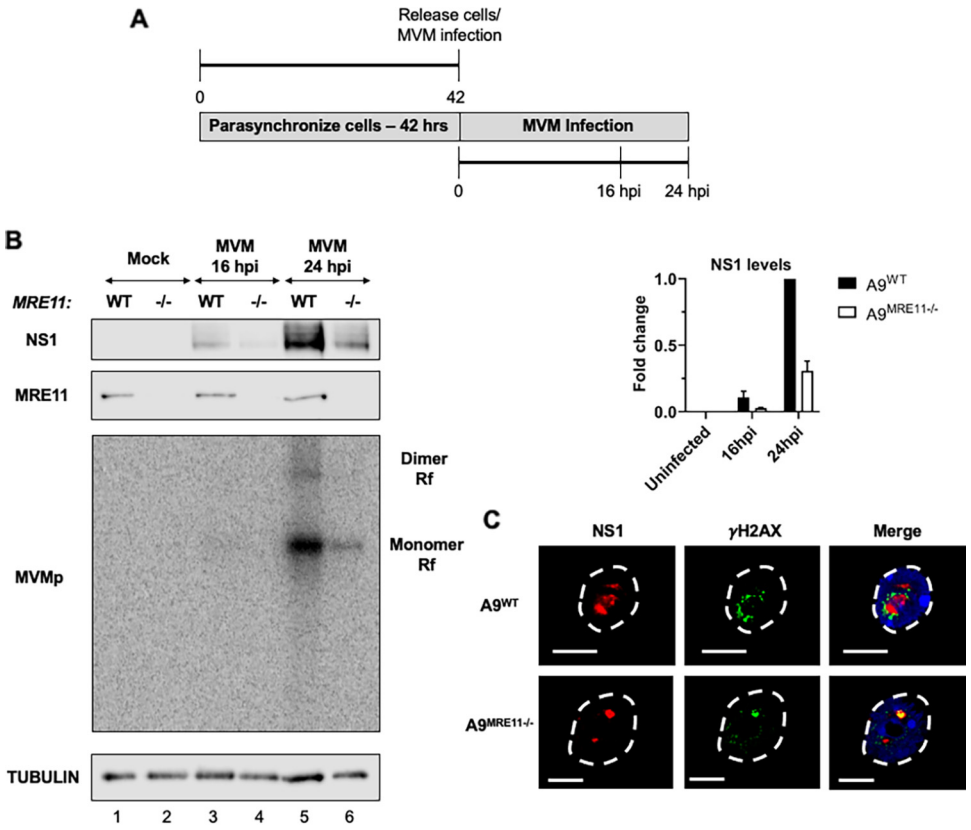

FIG 4 MVM expression and replication are diminished in MRE11-deficient cells. (A) Schematic illustrating the experimental procedure for MVM infection in panels B and C. (B) Murine A9 cells were transduced with a lentiviral construct that inducibly expressed CRISPR/Cas9 to create an MRE11-deficient stable cell line. Wild-type A9 control cells ($A9^{WT}$) and MRE11-deficient cells ($A9^{MRE11-/-}$) were infected at the time of release at an MOI of 10 before harvest at 16 hpi and 24 hpi. Western blotting was performed with antibodies against the indicated proteins. Southern blotting was performed with an MVMp genomic probe. The top right panel quantifies the NS1 band intensity from at least 3 independent biological replicates. (C) Wild-type and MRE11-deficient murine A9 cells were infected with MVM at an MOI of 10 for 16 h before being preextracted with cytoskeletal buffer and processed for IF using antibodies against NS1 and MRE11. The blue signal indicates DAPI staining, nuclear borders are demarcated by broken white lines, and the scale bar measures 5 μm.

MVM expression and replication are diminished in MRE11-deficient cells. To determine whether MRE11 is essential for MVM replication, we generated clonal MRE11-deficient A9 fibroblasts by targeting the *Mre11a* gene region using guide RNAs and inducible CRISPR/Cas9 driven from a lentiviral vector (45). As shown in Fig. 4B, MVM replicated slowly in MRE11-deficient A9 cells at 16 hpi and 24 hpi during synchronous infection compared with parental A9 cells, as monitored by levels of stable NS1 and viral genome copies. It is noteworthy that MVM replication was not completely arrested in these cells, suggesting the presence of additional redundant mechanisms that facilitate MVM replication. We validated these findings independently in additional MRE11-deficient A9 cells generated using independent guide RNAs (Fig. S1D; labeled $A9^{MRE11-/-\ \#2}$). Interestingly, APAR body imaging in MRE11-deficient A9 cells revealed that the NS1 foci were smaller (Fig. 4C, bottom panels), but the cellular DDR staining revealed the presence of γH2AX foci formed distinctly around the viral replication centers (Fig. 4C, bottom panels). These γH2AX foci might be induced by redundant cellular mechanisms that detect DNA damage in the absence of MRN-dependent ATM activation, likely ATR or DNA-PK (3). These findings extended our observations with *Mre11a* RNAi knockdown (Fig. 3), confirming that MRE11 is required for efficient MVM replication. However, the continued detection of low levels of NS1- and MVM-replicating isoforms in MRE11-deficient cells indicated that redundant pathways that facilitate MVM replication are present in the host.

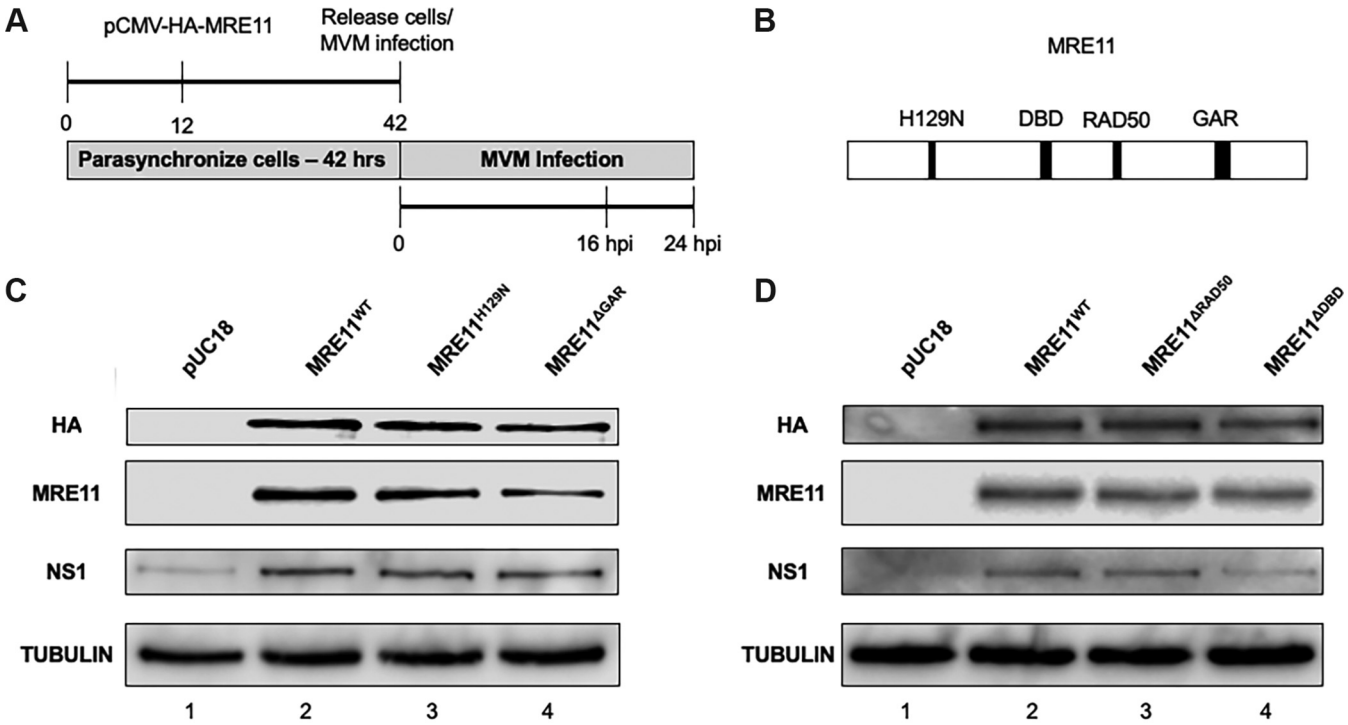

FIG 5 Ectopic MRE11 expression rescues MVM replication. (A) Schematic illustrating the experimental procedure for transfection of wild-type Mre11 expression vector into MRE11-deficient cells and infection with MVM in panels C and D. (B) Schematic of the MRE11 protein indicating the relative locations of the domains that had been mutated for rescue studies in panels C and D. MRE11-deficient murine A9 cells were transfected with a pUC18 control plasmid or a CMV-HA expression vector containing wild type and compared with expression of functional mutants of MRE11, such as H129N mutated (MRE11^{H129N}) and GAR mutated (MRE11$^{\Delta GAR}$) (C), and interaction mutants of MRE11, such as RAD50 interaction mutant (MRE11$^{\Delta RAD50}$) and DNA binding mutant (MRE11$^{\Delta DBD}$) (D) as depicted in panels A and B. Cells were then infected at an MOI of 10 before harvest at 16 hpi and 24 hpi. Western blotting was performed with antibodies against the indicated proteins, with HA and MRE11 being used to confirm transfection of the vector and stable ectopic protein expression. Tubulin was used as loading control.

Ectopic expression of MRE11 rescues MVM replication. To confirm the role of MRE11 in facilitating efficient MVM replication, we transfected a heterologous vector (*Mre11a*, cDNA cloned into cytomegalovirus-hemagglutinin [CMV-HA] expression vector) expressing wild-type (WT) *Mre11a* into the MRE11-deficient A9 cells (described above) prior to infection using the schematic shown in Fig. 5A and MRE11 mutant proteins schematized in Fig. 5B. We monitored the impact of rescuing MRE11 in these cells on MVM replication using NS1 Western blotting. Complementation with ectopic wild-type MRE11 tagged with HA, as well as MRE11 containing a point mutation (H129N; which abolishes its nuclease processing ability), was sufficient to rescue MVM replication (Fig. 5C, compare columns 1 to 3). The ability of MRE11^{H129N} to rescue MVM replication supports prior observations with the inhibitor Mirin, which diminishes the nuclease activity of MRE11 but does not impact MVM replication (17), further suggesting that neither the MRN complex nor DNA processing is required for MVM replication. Strikingly, the expression of ectopic MRE11, which does not possess the ability to bind DNA breaks due to the absence of its glycine- and arginine-rich (GAR) domain (46), was also sufficient to rescue MVM replication (Fig. 5C, column 4). This suggested that cellular MRE11 does not recognize the MVM genome as a DNA break substrate. Expression of MRE11 proteins that are incapable of interacting with RAD50 also rescued MVM replication (Fig. 5D, column 3, MRE11`$\sigma\upsilon\pi>\Delta$RAD50`$/\sigma\upsilon\pi>$ [47]), corroborating our ChIP-qPCR findings showing that RAD50 does not associate with MVM (Fig. 2C). However, MRE11 proteins lacking the ability to stably associate with DNA substrates due to a mutation in their 5′ DNA binding domain (MRE11`$\sigma\upsilon\pi>\Delta$DBD`$/\sigma\upsilon\pi>$ [48]) partially rescued MVM replication, suggesting the DNA binding activity of MRE11 is required for efficient MVM replication (Fig. 5D, column 4). Taken together, these findings confirmed that efficient MVM replication requires MRE11 in an MRN complex-independent manner.

DISCUSSION

In this study, we have discovered that the efficient replication of the autonomous protoparvovirus MVM requires the host DDR protein MRE11 on its P4 and P38 promoters. In the absence of MRE11, MVM replication, expression, and formation of viral replication centers are severely attenuated. Interestingly, MRE11 associates with the replicating MVM genome in an MRN complex-independent manner. These findings shed light on how MVM genomes evade degradation and transcriptional suppression by host cellular DDR pathways, making the biology of protoparvoviruses distinct from that of dependoparvoviruses.

The cellular DDR pathways are essential for the maintenance of host genome integrity, and it has become increasingly clear that they also regulate the permissiveness of host cells to infection by DNA viruses (8). As the principal complex driving the recognition of DNA breaks prior to DDR signal induction, the MRN complex serves as a rheostat that modulates the host responses to DNA breaks. The colocalization between the MRN complex and viral replication centers has been previously observed with SV40, polyomaviruses, AAV, and recombinant AAV vectors (12–14, 34–36). Imaging studies on MVM-APAR bodies have similarly discovered that MRN complex proteins and APAR body markers colocalize (17, 31). However, the functional role played by MRN complex proteins in the MVM life cycle has been unknown. Our studies highlight an MRN-independent role of MRE11 in facilitating efficient MVM replication and formation of nuclear viral replication centers. We have found that MRE11, but not RAD50 or NBS1, is associated with the viral genome. This observation precludes the possibility of MRN-mediated viral genome processing during MVM replication. Future studies will investigate the stepwise signals generated by MVM replication which inhibit the activation of cellular DDR signals in the viral genome. This local response is different from signals transduced globally in the host cell genome, made up of increasing DNA breaks and subsequent induction of γH2AX.

Studies on the transduction efficiency of self-complementary AAV (scAAV) vectors in patient-derived and mouse ATLD cells that are deficient in MRE11 have found that the absence of MRE11 facilitates efficient transgene expression (37). These findings initially suggested that MRE11, the MRN complex, and the eventual cellular DDR signals play an inhibitory role in the AAV/scAAV genome, which must be compensated by coinfected adenovirus E1B55K or E4orf6 to facilitate expression (10, 49). These findings are supported by discoveries that MRE11 associates with the inverted terminal repeats (ITR) which flank AAV/rAAV genomes (22, 50). This interaction might also facilitate the concatemerization of AAV genomes in their nonreplicative state to form extrachromosomal viral episomes (51–53). However, the requirement of AAV replication on helper virus coinfection complicates the dissection of parvovirus-specific DDR signals. In striking contrast, we have found that the absence of MRE11 by knockdown or genetic knockout using CRISPR/Cas9 leads to a decrease in MVM replication, suggesting that MVM possesses distinct pathways to interact with DDR sensors like MRE11. We speculate that this requirement of MRE11 for efficient replication might be a unique mechanism evolved by autonomous parvoviruses to facilitate their life cycles in host cells without the aid of helper viruses. We have additionally found that MRE11 associates with MVM in the viral promoters under conditions of virus replication, remaining distinct from the heterotelomeric left-hand and right-hand ends. This localization to MVM promoters, rather than MVM ITRs, might also explain the absence of intermolecular recombination between MVM genomes, making autonomous parvoviruses distinct from dependoparvoviruses (33, 39).

Interestingly, the absence of MRE11 in the plasmid-based expressing viral genomes (MVMp FD) suggests that MVM expression is not sufficient to facilitate MRE11 recruitment. This recruitment might require both replication and expression events in the same virus molecule, likely driven by the formation of single-stranded and double-stranded genomic intermediates or by the formation of NS1-induced nick during genome amplification (54–58). Upon recruitment to host DDR sites in the host genome, MRE11 plays a role in

processing the broken DNA through its nuclease domain (59). However, during MVM infection, the inability of the MRN nuclease inhibitor Mirin to attenuate virus replication (17) or the complete rescue of virus replication by the overexpression of MRE11^{H129N} mutant suggests that MRE11 does not process the MVM genome. Additionally, the ectopic MRE11 mutants that are incapable of binding to cellular DNA double-strand breaks (MRE11$^{\Delta GAR}$ [46]) or associating with RAD50 (MRE11$^{\Delta RAD50}$ [47]) are sufficient to rescue MVM replication. These observations further suggest that the MVM genome and cellular DNA breaks are dissimilar. In this regard, structural studies on the DNA binding interface of MRE11 have found that MRE11 molecules, which are bound to two-ended DNA, generate a symmetric complex, which is distinct from MRE11 molecules bound to one-ended DNA, forming an asymmetric complex (1, 60). From these structural studies, we speculate that the dimerization and nuclease activities of MRE11 in the replicating MVM genome are distinct from those that initiate the repair of cellular double-strand breaks. Consistent with this assertion, we have found that ectopic MRE11 mutants that are incapable of binding to DNA molecules (MRE11$^{\Delta DBD}$ [48]) partially rescue MVM replication. This suggests that the proviral role of MRE11 in regulating the MVM life cycle is partially dependent on its DNA binding function and independent of its DNA end-processing activity.

ChIP sequencing (ChIP-seq) studies of MRN complex proteins in the human genome have recently found that MRE11, RAD50, and NBS1 are associated with the promoters of actively transcribing genes, suggesting their involvement in protecting the host genome from transcription-induced DNA damage (61). This predilection of MRN complex proteins for active promoter regions might be a result of open chromatin associated with transcriptionally active promoters, which generate local DNA breaks and subsequently recruit MRN complex proteins. However, in the MVM genome, only MRE11 is concentrated in the P4 and P38 promoter regions. In this regard, recent studies have discovered that MRE11 associates with the host chromatin remodeling enzyme lysine-specific histone demethylase 1 (LSD1) (62). It is therefore possible that MRE11 recruitment to the MVM promoters facilitates the opening of local chromatin, regulating NS1 and NS2 gene expression and, eventually, virus replication.

In contrast to the presence of MRE11 on the MVM promoters, the recruitment of DDR proteins to the host genome leads to transcriptional repression of the chromatin surrounding the break site to prevent erroneous effects of expressing proteins from a break-associated locus. Consistent with this model, it is expected that lytic DNA viruses, which express and replicate vigorously in the host nucleus, would inhibit the formation of transcriptionally repressive DDR-associated marks in the viral genome. Adenovirus is the poster child for this process, expressing E1B55K and E4orf6, which degrade and mislocalize MRE11, respectively, contributing to the lack of local γH2AX in the adenovirus genome (9, 10). However, MVM, by virtue of its limited coding capacity, does not express proteins that impact host cell MRE11 levels. Characterization of the global changes in cellular MRE11 levels during MVM infection has previously revealed that MRE11 proteins are degraded in a proteosome-dependent manner as infection progresses (17). However, this decrease in MRE11 levels occurs at 30 hpi or later, suggesting an active role of MVM in targeting the cellular sensors of DNA damage for its own benefit. In contrast, the requirement of MRE11 for efficient replication early in infection suggests that the MVM life cycle in the host cell is biphasic, consisting of the early phase, which is dependent on MRE11, and the late phase, which is independent of MRE11. It is also possible that depletion of MRE11 at late stages of viral infection facilitates efficient host cell degradation. However, the signals that separate MRE11-dependent from MRE11-independent signals during MVM infection remain unknown.

Regardless of early or late stages of infection, complete γH2AX signals do not form in the MVM genome, consistent with its vigorously expressing and replicating life cycle in the nucleus (16, 41). In support of these findings, the DDR transducer upstream of γH2AX, MDC1, also remains distinct from MVM APAR bodies, likely associating with the host DDR sites (31). However, the result of γH2AX signals is to recruit the ATM kinase to the cellular DDR site, which is required for efficient MVM replication (3, 17). The dependence of MVM on MRE11 binding for efficient replication likely suggests that the MVM genome does not

require direct signals from the ATM kinase. Instead, we speculate that ATM likely plays a role in signaling host cell DDR sites by phosphorylating H2AX subunits, marking them as regions for the establishment of MVM-APAR bodies.

It is noteworthy that MVM replication still progresses slowly in cells where MRE11 is knocked out by CRISPR/Cas9. This suggests that there are alternate compensatory pathways that can be usurped by MVM to replicate in the absence of MRE11, such as EXO1, involved in compensating replication fork protection in the absence of MRE11 (63). Importantly, this is a key evolutionary feature of autonomous parvoviruses, reflecting their ability to adapt to changes in the nuclear environment to benefit the viral life cycle. If MVM replication was solely dependent on MRE11 binding, it is likely that these autonomous parvoviruses would have died out. It is noteworthy that even in the absence of MRE11, the smaller viral replication centers are associated with cellular sites of DNA damage marked by γH2AX. The host cell deploys compensatory pathways such as the related PI3 kinase-related kinases ATR and DNA-PK to phosphorylate H2AX subunits in the absence of ATM activation (64, 65). It is possible that some of these pathway proteins, many of which colocalize with MVM-APAR bodies, compensate for the absence of MRE11 to facilitate the formation of viral replication centers in the nucleus. These observations suggest that MRE11 is not required for the MVM genome to localize to, or usurp factors from, host DDR sites. Therefore, the machinery regulating the localization of the viral genome and those required to efficiently replicate the virus are distinct from one another.

MATERIALS AND METHODS

Cell lines, virus, and viral infection. Male murine A9 fibroblasts, male murine NIH 3T3 embryonic fibroblasts, human 324K kidney cells, female human U2OS osteosarcoma cells, and female human embryonic kidney 293T cells were maintained in Dulbecco's modified Eagle's medium (DMEM; high glucose; Gibco) supplemented with 5% Serum Plus (Sigma-Aldrich) and 50 μg/mL gentamicin (Gibco). Cells were cultured in 5% CO_2 at 37°C. Cell lines are routinely authenticated for mycoplasma contamination and background levels of DNA damage by γH2AX staining.

MVMp virus was produced in A9 and 324K cells as described previously. MVMp infection was carried out at a multiplicity of infection (MOI) of 10 unless otherwise noted. Lentiviruses for the generation of MRE11-deficient A9 cells were produced in HEK-293T cells by transiently transfecting equimolar amounts of the lentiviral vector, empty HIV Gag/Pol, and vesicular stomatitis virus envelope (VSV-G)-expressing constructs using LipoD293 (SignaGen Laboratories) for 48 h. Lentiviral particles were collected and inactivated by freeze-thaw cycle at −80°C before being used to transduce A9 target cells. Stable doxycycline-inducible A9 cells were selected with 6 μg/mL of puromycin for 1 week, and lentivirus-transformed cell lines were induced with 500 ng/mL of doxycycline hydrochloride (MP Biomedicals) for 5 days before being subcloned by limiting dilution, screening, and expanding out the population.

Plasmids, siRNA, and transfections. The Mre11a open reading frame (ORF) was cloned into the CMV-HA expression vector (Clontech) using EcoRI and KpnI restriction enzyme digestion. MRE11^{H129N}, MRE11$^{\Delta GAR}$, MRE11$^{\Delta RAD50}$, and MRE11$^{\Delta DBD}$ mutations were generated in the vector backbone using PCR-directed mutagenesis (see Table 1). Mouse siMre11a 1 (catalog no. AM16708; siRNA ID 156974), mouse siMre11a 2 (catalog no. AM16708; siRNA ID 156975), human siMre11a (catalog no. 4390824; siRNA ID s8959), and negative-control (catalog no. AM4635) siRNAs were purchased from Thermo Scientific. Lentivirus constructs designed to inducibly express CRISPR/Cas9 (TLCV2) were obtained from Addgene (45), and the mouse Mre11a guide RNA was cloned into it using BbsI as described previously (16). Lentivirus constructs designed to inducibly express the Mre11a guide VSV-G and the Mre11a-guide RNA-containing TLCV2 construct into 293T cells for 48 h.

Antibodies. Antibodies used for Western blot analysis were tubulin (MilliporeSigma; clone DM1A; catalog no. 05-829), NS1 (2C9b monoclonal antibody), MRE11 (Cell Signaling; catalog no. 4895S), HA (Cell Signaling; catalog no. 3724S), horseradish peroxidase (HRP)-conjugated anti-mouse secondary antibody (Cell Signaling; catalog no. 7076S), and HRP-conjugated anti-rabbit secondary antibody (Cell Signaling; catalog no. 7074S).

Antibodies used for immunofluorescence analysis were MRE11 (Cell Signaling; catalog no. 4895S), NBS1 (Cell Signaling; catalog no. 14956S), RAD50 (Cell Signaling; catalog no. 3427S), NS1 (2C9b monoclonal antibody), Alexa Fluor 568-conjugated anti-mouse secondary antibody (Thermo Scientific; catalog no. A11004), and Alexa Fluor-conjugated anti-rabbit secondary antibody (Thermo Scientific; catalog no. A11008).

Antibodies used for ChIP-qPCR analysis were MRE11 (Cell Signaling; catalog no. 4895S), NBS1 (Cell Signaling; catalog no. 14956S), and RAD50 (Cell Signaling; catalog no. 3427S).

Southern blot analysis. Cells were harvested at the indicated time points, pelleted, and resuspended in southern lysis buffer (2% SDS, 0.15 M sodium chloride, 10 mM Tris, pH 8, and 1 mM EDTA). The lysed extracts were proteinase K (NEB) treated overnight at 37°C before genomic DNA was sheared with 25-gauge by 5/8-in. 1-mL needle syringe (BD Biosciences). Total DNA content was quantified on a NanoDrop spectrophotometer, and equal amounts of DNA were loaded per well and electrophoresed

TABLE 1 Primers used in this study

Primer name	5′–3′ sequence
P4 ChIP primer (F)	TGATAAGCGGTTCAGGGAGT
P4 ChIP primer (R)	CCAGCCATGGTTAGTTGGTT
P38 ChIP primer (F)	CCGAAAAGTACGCCTCTCAG
P38 ChIP primer (R)	CCGCAACAGGAGTATTTGGT
NS1-ORF ChIP primer (F)	AACCTCACCAGAGGACTGGA
NS1-ORF ChIP primer (R)	TGCTGTTTTGGTTCTGGCTA
VP-ORF ChIP primer (F)	ACGAAAATCAAGAAGGCACAG
VP-ORF ChIP primer (R)	ACGAAAATCAAGAAGGCACAG
RHE ChIP primer (F)	GGTTGGTTGCTCTGCTCAA
RHE ChIP primer (R)	ACCAACCAGACCGGCTTT
Mre11a gRNA 1 (F)	CACCGTTGCCGTGGATACTAAATAC
Mre11a gRNA 1 (R)	AAACGTATTTAGTATCCACGGCAAC
Mre11a gRNA 2 (F)	CACCGCGGGCACAACATCTAGCAAA
Mre11a gRNA 2 (R)	AAACTTTGCTAGATGTTGTGCCCGC
H129N mutagenesis PCR (F)	TGGCAATAATGACGATCCCACA
H129N mutagenesis PCR (R)	ATCGTCATTATTGCCATGAATACT
Delta RAD50 mutagenesis PCR (F)	GCGAAGCAGATGCCATCGAGGAATTAGTGAAG
Delta RAD50 mutagenesis PCR (R)	TGGCATCTGCTTCGCCCATCCCTCTTTC
Delta DBD mutagenesis PCR (F)	GAAAAACATCAGAAGGAGCAACGCTTAGAG
Delta DBD mutagenesis PCR (R)	CTTCTGATGTTTTTCCCTTTTGTTCCCTGTGC
Delta GAR mutation gene block	CGAGAGGCCATGAGCAGAGCCCGGGCCCTCAGATCAC AGTCAGAGACCTCCACCTCAGCCTTTAGTGCTGAGGAC CTGAGCTTTGATACATCGGAGCAGACAGCAAATGACTC TGATGACAGCCTGTCAGCAGTGCCGAGCAGACAGAGCT CGGCACCTAGAGGAGGCTC

on a 1% agarose gel at 33 V overnight. DNA was transferred to a nitrocellulose membrane and hybridized with homologous genomic clones of MVMp. The MVMp probe was generated by agarose gel extraction and purification (Qiagen) of BamHI-XbaI double-digested MVMp infectious clone.

Western blot analysis. Cell pellets were lysed on ice for 10 min in radioimmunoprecipitation assay (RIPA) buffer. The lysate was pelleted by centrifugation for 10 min at 10,000 $\times$ *g* at 4°C. The protein sample concentration was calculated using bicinchoninic acid (BCA) assay (Bio-Rad).

Immunofluorescence analysis. MVMp-infected A9 cells were harvested at the indicated time points by preextracting with CSK buffer {10 mM PIPES [piperazine-*N*,*N*′-bis(2-ethanesulfonic acid)], pH 6.8, 100 mM sodium chloride, 300 mM sucrose, 1 mM EGTA, and 1 mM magnesium chloride} for 3 min followed by CSK buffer with 0.5% Triton X-100 for 3 min. Cells were cross-linked with 4% paraformaldehyde for 10 min at room temperature, washed with phosphate-buffered saline (PBS), and permeabilized with 0.5% Triton X-100 in PBS for 10 min. The samples were blocked with 3% BSA in PBS for 30 min, incubated with the indicated primary antibodies for 30 min, and incubated with the indicated secondary antibodies for 30 min. Samples were washed with PBS between treatments and, finally, mounted with Fluoromount solution containing DAPI (4′,6-diamidino-2-phenylindole; SouthernBiotech).

For high-salt perfusion experiments coupled with confocal imaging, cells were preextracted in CSK and CSK with 0.5% Triton X-100 as described above before being perfused with 150 mM sodium chloride in PBS solution for 3 min before being permeabilized and processed for imaging as described above. The salt extraction procedure was modified and optimized from previously described studies in human papillomavirus (HPV) (66).

Distance analysis. Immunofluorescence imaging was performed on the samples described above using a Leica Stellaris 5 DMi8 confocal microscope. Confocal z-stacks of the viral replication centers (monitored by NS1 staining) and cellular DDR foci (monitored by staining for MRE11, RAD50, or NBS1) were acquired using a 63$\times$ oil lens objective. The images were analyzed using Fiji software. Background noise was filtered out using the Kalman stack filter plugin to determine the center of maximum intensity of the imaged foci. The x-y-z coordinates of the viral and cellular foci were calculated using the Sync Measure 3D plugin in the Fiji software suite. The three-dimensional distance between these foci was calculated by computing the displacement vector between the two locations, as described previously (16).

Isolation of MVMp nucleoprotein complexes. MVMp nucleoprotein complexes were extracted from infected A9 cells as previously described (41). Cells were washed with phosphate-buffered saline (PBS) before they were collected with HBE buffer (10 mM HEPES, 5 mM KCl, and 1 mM EDTA) into Eppendorf tubes. Samples were centrifuged at 1,000 $\times$ *g* for 3 min at room temperature, aspirated, and resuspended in 500 μL HBE. Cells were lysed on ice for 10 min by the addition of 1% NP-40 (to a final concentration of 0.1%). The nuclei were pelleted by centrifugation for 5 min at 1,000 $\times$ *g*. The supernatant (cytoplasmic extract) was transferred to a new tube, and the nuclei (pellet) were resuspended in 500 μL HBE. Sodium chloride (NaCl) was added to the suspension at a final concentration of 200 mM and incubated on ice for 2 h. The chromatin was pelleted at 10,000 $\times$ *g* for 10 min, and the supernatant containing viral nucleoprotein complexes was isolated for ChIP-qPCR analysis (described below).

ChIP-qPCR. MVMp nucleoprotein complexes were cross-linked in 0.1% formaldehyde, and MVM-infected A9 cells were cross-linked in 1% formaldehyde for 10 min at room temperature. The cross-linking reactions were quenched in 0.125 M glycine. Cells were lysed in ChIP lysis buffer (1% SDS, 10 mM EDTA, 50 mM Tris-HCl, pH 8, and protease inhibitor) for 20 min on ice, and the cell lysates were sonicated using a Diagenode Bioruptor Pico for 60 cycles (30 s on and 30 s off per cycle), before being incubated overnight at 4°C with the antibodies bound to protein A Dynabeads (Invitrogen). The MVMp-nucleoprotein complexes, which had been cross-linked and quenched, were purified using 3K Amicon centrifugal filter units (Millipore) and purified into PBS as previously described (41). This was added to the antibody-Dynabead conjugate overnight. All ChIP samples were washed for 3 min each at 4°C with low-salt wash (0.01% SDS, 1% Triton X-100, 2 mM EDTA, 20 mM Tris-HCl, pH 8, and 150 mM NaCl), high-salt wash (0.01% SDS, 1% Triton X-100, 2 mM EDTA, 20 mM Tris-HCl, pH 8, and 500 mM NaCl), lithium chloride wash (0.25 M LiCl, 1% NP-40, 1% deoxycholate [DOC], 1 mM EDTA, and 10 mM Tris-HCl, pH 8) and twice with Tris-EDTA (TE) buffer. Samples were eluted with SDS elution buffer (1% SDS, 0.1 M sodium bicarbonate), and cross-links were reversed using 0.2 M NaCl and proteinase K (NEB) and incubated at 56°C overnight. DNA was purified using PCR purification kit (Qiagen) and eluted in 100 μL of buffer EB (Qiagen). ChIP DNA was quantified by qPCR analysis (Bio-Rad) under the following conditions: 95°C for 5 min, 95°C for 10 s, and 60°C for 30 s for 40 cycles.

Cell cycle analysis. Cell cycle analysis was performed by staining total DNA content with propidium iodide staining (Sigma-Aldrich). A9 cells were harvested, washed in 1 mL of PBS, resuspended in 300 μL of PBS, and fixed with 700 μL of chilled 100% ethanol for 1 h at 4°C. Samples were resuspended in 300 μL of PBS, treated with RNase for 1 h at 37°C, and incubated with 5 μL propidium iodide. Cells were analyzed on a BD Accuri fluorescence-activated cell sorter (FACS) machine (University of Wisconsin-Biophysics Instrumentation Facility) on the FL2 channel.

SUPPLEMENTAL MATERIAL

Supplemental material is available online only.

SUPPLEMENTAL FILE 1, PDF file, 0.1 MB.

ACKNOWLEDGMENTS

We acknowledge expert technical guidance from Ephraim Leigl (IMV) and Marchel Hill (Palmenberg Lab; IMV); MegAnn Haubold (Majumder Lab; IMV) for critical reading of the manuscript.

K.M. is supported by funding from the OVCRGE, SMPH, Wisconsin Partnership Program, and UW-CCC and an NIH-K99/R00 Pathway to Independence award (AI148511). J.N.P.A. is supported by an NSF-GRFP award (2018238648) and a SciMed GRS Fellowship from the University of Wisconsin—Madison. I.K.J. was partially supported by a Sophomore Research Fellowship from the University of Wisconsin—Madison.

We declare no competing financial interests.

REFERENCES

1. Syed A, Tainer JA. 2018. The MRE11–RAD50–NBS1 complex conducts the orchestration of damage signaling and outcomes to stress in DNA replication and repair. Annu Rev Biochem 87:263–294. https://doi.org/10.1146/annurev-biochem-062917-012415.
2. Burma S, Chen BP, Murphy M, Kurimasa A, Chen DJ. 2001. ATM phosphorylates histone H2AX in response to DNA double-strand breaks. J Biol Chem 276:42462–42467. https://doi.org/10.1074/jbc.C100466200.
3. Blackford AN, Jackson SP. 2017. ATM, ATR, and DNA-PK: the trinity at the heart of the DNA damage response. Mol Cell 66:801–817. https://doi.org/10.1016/j.molcel.2017.05.015.
4. Rogakou EP, Pilch DR, Orr AH, Ivanova VS, Bonner WM. 1998. DNA double-stranded breaks induce histone H2AX phosphorylation on serine 139. J Biol Chem 273:5858–5868. https://doi.org/10.1074/jbc.273.10.5858.
5. Shanbhag NM, Rafalska-Metcalf IU, Balane-Bolivar C, Janicki SM, Greenberg RA. 2010. ATM-dependent chromatin changes silence transcription in cis to DNA double-strand breaks. Cell 141:970–981. https://doi.org/10.1016/j.cell.2010.04.038.
6. Kakarougkas A, Ismail A, Chambers AL, Riballo E, Herbert AD, Künzel J, Löbrich M, Jeggo PA, Downs JA. 2014. Requirement for PBAF in transcriptional repression and repair at DNA breaks in actively transcribed regions of chromatin. Mol Cell 55:723–732. https://doi.org/10.1016/j.molcel.2014.06.028.
7. Iannelli F, Galbiati A, Capozzo I, Nguyen Q, Magnuson B, Michelini F, D'Alessandro G, Cabrini M, Roncador M, Francia S, Crosetto N, Ljungman M, Carninci P, d'Adda di Fagagna F. 2017. A damaged genome's transcriptional landscape through multilayered expression profiling around in situ-mapped DNA double-strand breaks. Nat Commun 8:15656. https://doi.org/10.1038/ncomms15656.
8. Pancholi NJ, Price AM, Weitzman MD. 2017. Take your PIKK: tumour viruses and DNA damage response pathways. Philos Trans R Soc Lond B Biol Sci 372:20160269. https://doi.org/10.1098/rstb.2016.0269.
9. Shah GA, O'Shea CC. 2015. Viral and cellular genomes activate distinct DNA damage responses. Cell 162:987–1002. https://doi.org/10.1016/j.cell.2015.07.058.
10. Stracker TH, Carson CT, Weitzman MD. 2002. Adenovirus oncoproteins inactivate the Mre11–Rad50–NBS1 DNA repair complex. Nature 418:348–352. https://doi.org/10.1038/nature00863.
11. Evans JD, Hearing P. 2005. Relocalization of the Mre11-Rad50-Nbs1 complex by the adenovirus E4 ORF3 protein is required for viral replication. J Virol 79:6207–6215. https://doi.org/10.1128/JVI.79.10.6207-6215.2005.
12. Dahl J, You J, Benjamin TL. 2005. Induction and utilization of an ATM signaling pathway by polyomavirus. J Virol 79:13007–13017. https://doi.org/10.1128/JVI.79.20.13007-13017.2005.
13. Shi Y, Dodson GE, Shaikh S, Rundell K, Tibbetts RS. 2005. Ataxia-telangiectasia-mutated (ATM) is a T-antigen kinase that controls SV40 viral replication in vivo. J Biol Chem 280:40195–40200. https://doi.org/10.1074/jbc.C500400200.
14. Zhao X, Madden-Fuentes RJ, Lou BX, Pipas JM, Gerhardt J, Rigell CJ, Fanning E. 2008. Ataxia telangiectasia-mutated damage-signaling kinase- and proteasome-dependent destruction of Mre11-Rad50-Nbs1 subunits in simian virus 40-infected primate cells. J Virol 82:5316–5328. https://doi.org/10.1128/JVI.02677-07.

15. Majumder K, Boftsi M, Whittle FB, Wang J, Fuller MS, Joshi T, Pintel DJ. 2020. The NS1 protein of the parvovirus MVM aids in the localization of the viral genome to cellular sites of DNA damage. PLoS Pathog 16: e1009002. https://doi.org/10.1371/journal.ppat.1009002.
16. Majumder K, Wang J, Boftsi M, Fuller MS, Rede JE, Joshi T, Pintel DJ. 2018. Parvovirus minute virus of mice interacts with sites of cellular DNA damage to establish and amplify its lytic infection. Elife 7:e37750. https://doi.org/10.7554/eLife.37750.
17. Adeyemi RO, Landry S, Davis ME, Weitzman MD, Pintel DJ. 2010. Parvovirus minute virus of mice induces a DNA damage response that facilitates viral replication. PLoS Pathog 6:e1001141. https://doi.org/10.1371/journal.ppat.1001141.
18. Adeyemi RO, Pintel DJ. 2014. The ATR signaling pathway is disabled during infection with the parvovirus minute virus of mice. J Virol 88: 10189–10199. https://doi.org/10.1128/JVI.01412-14.
19. Adeyemi RO, Fuller MS, Pintel DJ. 2014. Efficient parvovirus replication requires CRL4Cdt2-targeted depletion of p21 to prevent its inhibitory interaction with PCNA. PLoS Pathog 10:e1004055. https://doi.org/10.1371/journal.ppat.1004055.
20. Adeyemi RO, Pintel DJ. 2014. Parvovirus-induced depletion of cyclin B1 prevents mitotic entry of infected cells. PLoS Pathog 10:e1003891. https://doi.org/10.1371/journal.ppat.1003891.
21. Adeyemi RO, Pintel DJ. 2012. Replication of minute virus of mice in murine cells is facilitated by virally induced depletion of p21. J Virol 86: 8328–8332. https://doi.org/10.1128/JVI.00820-12.
22. Cotmore SF, Tattersall P. 2014. Parvoviruses: small does not mean simple. Annu Rev Virol 1:517–537. https://doi.org/10.1146/annurev-virology-031413-085444.
23. Willwand K, Mumtsidu E, Kuntz-Simon G, Rommelaere J. 1998. Initiation of DNA replication at palindromic telomeres is mediated by a duplex-to-hairpin transition induced by the minute virus of mice nonstructural protein NS1. J Biol Chem 273:1165–1174. https://doi.org/10.1074/jbc.273.2.1165.
24. Baldauf AQ, Willwand K, Mumtsidu E, Nüesch JP, Rommelaere J. 1997. Specific initiation of replication at the right-end telomere of the closed species of minute virus of mice replicative-form DNA. J Virol 71:971–980. https://doi.org/10.1128/JVI.71.2.971-980.1997.
25. Naeger LK, Cater J, Pintel DJ. 1990. The small nonstructural protein (NS2) of the parvovirus minute virus of mice is required for efficient DNA replication and infectious virus production in a cell-type-specific manner. J Virol 64:6166–6175. https://doi.org/10.1128/JVI.64.12.6166-6175.1990.
26. Tullis GE, Labieniec-Pintel L, Clemens KE, Pintel D. 1988. Generation and characterization of a temperature-sensitive mutation in the NS-1 gene of the autonomous parvovirus minute virus of mice. J Virol 62:2736–2744. https://doi.org/10.1128/JVI.62.8.2736-2744.1988.
27. Cotmore SF, Gottlieb RL, Tattersall P. 2007. Replication initiator protein NS1 of the parvovirus minute virus of mice binds to modular divergent sites distributed throughout duplex viral DNA. J Virol 81:13015–13027. https://doi.org/10.1128/JVI.01703-07.
28. Bashir T, Rommelaere J, Cziepluch C. 2001. In vivo accumulation of cyclin A and cellular replication factors in autonomous parvovirus minute virus of mice-associated replication bodies. J Virol 75:4394–4398. https://doi.org/10.1128/JVI.75.9.4394-4398.2001.
29. Young PJ, Jensen KT, Burger LR, Pintel DJ, Lorson CL. 2002. Minute virus of mice NS1 interacts with the SMN protein, and they colocalize in novel nuclear bodies induced by parvovirus infection. J Virol 76:3892–3904. https://doi.org/10.1128/jvi.76.8.3892-3904.2002.
30. Cziepluch C, Lampel S, Grewenig A, Grund C, Lichter P, Rommelaere J. 2000. H-1 parvovirus-associated replication bodies: a distinct virus-induced nuclear structure. J Virol 74:4807–4815. https://doi.org/10.1128/jvi.74.10.4807-4815.2000.
31. Ruiz Z, Mihaylov IS, Cotmore SF, Tattersall P. 2011. Recruitment of DNA replication and damage response proteins to viral replication centers during infection with NS2 mutants of minute virus of mice (MVM). Virology 410:375–384. https://doi.org/10.1016/j.virol.2010.12.009.
32. Luo Y, Qiu J. 2013. Parvovirus infection-induced DNA damage response. Future Virol 8:245–257. https://doi.org/10.2217/fvl.13.5.
33. Tattersall P, Ward DC. 1976. Rolling hairpin model for replication of parvovirus and linear chromosomal DNA. Nature 263:106–109. https://doi.org/10.1038/263106a0.
34. Schwartz RA, Palacios JA, Cassell GD, Adam S, Giacca M, Weitzman MD. 2007. The Mre11/Rad50/Nbs1 complex limits adeno-associated virus transduction and replication. J Virol 81:12936–12945. https://doi.org/10.1128/JVI.01523-07.
35. Cervelli T, Palacios JA, Zentilin L, Mano M, Schwartz RA, Weitzman MD, Giacca M. 2008. Processing of recombinant AAV genomes occurs in specific nuclear structures that overlap with foci of DNA-damage-response proteins. J Cell Sci 121:349–357. https://doi.org/10.1242/jcs.003632.
36. Millet R, Jolinon N, Nguyen XN, Berger G, Cimarelli A, Greco A, Bertrand P, Odenthal M, Büning H, Salvetti A. 2015. Impact of the MRN complex on adeno-associated virus integration and replication during coinfection with herpes simplex virus 1. J Virol 89:6824–6834. https://doi.org/10.1128/JVI.00171-15.
37. Lentz TB, Samulski RJ. 2015. Insight into the mechanism of inhibition of adeno-associated virus by the Mre11/Rad50/Nbs1 complex. J Virol 89: 181–194. https://doi.org/10.1128/JVI.01990-14.
38. Hashiguchi K, Matsumoto Y, Yasui A. 2007. Recruitment of DNA repair synthesis machinery to sites of DNA damage/repair in living human cells. Nucleic Acids Res 35:2913–2923. https://doi.org/10.1093/nar/gkm115.
39. Tullis G, Schoborg RV, Pintel DJ. 1994. Characterization of the temporal accumulation of minute virus of mice replicative intermediates. J Gen Virol 75:1633–1646. https://doi.org/10.1099/0022-1317-75-7-1633.
40. Stracker TH, Petrini JH. 2011. The MRE11 complex: starting from the ends. Nat Rev Mol Cell Biol 12:90–103. https://doi.org/10.1038/nrm3047.
41. Boftsi M, Majumder K, Burger LR, Pintel DJ. 2020. Binding of CCCTC-binding factor (CTCF) to the minute virus of mice genome is important for proper processing of viral P4-generated pre-mRNAs. Viruses 12:1368. https://doi.org/10.3390/v12121368.
42. Deleu L, Pujol A, Faisst S, Rommelaere J. 1999. Activation of promoter P4 of the autonomous parvovirus minute virus of mice at early S phase is required for productive infection. J Virol 73:3877–3885. https://doi.org/10.1128/JVI.73.5.3877-3885.1999.
43. Maser RS, Mirzoeva OK, Wells J, Olivares H, Williams BR, Zinkel RA, Farnham PJ, Petrini JH. 2001. Mre11 complex and DNA replication: linkage to E2F and sites of DNA synthesis. Mol Cell Biol 21:6006–6016. https://doi.org/10.1128/MCB.21.17.6006-6016.2001.
44. Vogel R, Seyffert M, Strasser R, de Oliveira AP, Dresch C, Glauser DL, Jolinon N, Salvetti A, Weitzman MD, Ackermann M, Fraefel C. 2012. Adeno-associated virus type 2 modulates the host DNA damage response induced by herpes simplex virus 1 during coinfection. J Virol 86:143–155. https://doi.org/10.1128/JVI.05694-11.
45. Barger CJ, Branick C, Chee L, Karpf AR. 2019. Pan-cancer analyses reveal genomic features of FOXM1 overexpression in cancer. Cancers (Basel) 11: 251. https://doi.org/10.3390/cancers11020251.
46. Déry U, Coulombe Y, Rodrigue A, Stasiak A, Richard S, Masson JY. 2008. A glycine-arginine domain in control of the human MRE11 DNA repair protein. Mol Cell Biol 28:3058–3069. https://doi.org/10.1128/MCB.02025-07.
47. Lammens K, Bemeleit DJ, Möckel C, Clausing E, Schele A, Hartung S, Schiller CB, Lucas M, Angermüller C, Söding J, Strässer K, Hopfner KP. 2011. The Mre11:Rad50 structure shows an ATP-dependent molecular clamp in DNA double-strand break repair. Cell 145:54–66. https://doi.org/10.1016/j.cell.2011.02.038.
48. Arthur LM, Gustausson K, Hopfner KP, Carson CT, Stracker TH, Karcher A, Felton D, Weitzman MD, Tainer J, Carney JP. 2004. Structural and functional analysis of Mre11-3. Nucleic Acids Res 32:1886–1893. https://doi.org/10.1093/nar/gkh343.
49. Schwartz RA, Lakdawala SS, Eshleman HD, Russell MR, Carson CT, Weitzman MD. 2008. Distinct requirements of adenovirus E1b55K protein for degradation of cellular substrates. J Virol 82:9043–9055. https://doi.org/10.1128/JVI.00925-08.
50. Cotmore SF, Tattersall P. 2013. Parvovirus diversity and DNA damage responses. Cold Spring Harb Perspect Biol 5:a012989. https://doi.org/10.1101/cshperspect.a012989.
51. Duan D, Sharma P, Yang J, Yue Y, Dudus L, Zhang Y, Fisher KJ, Engelhardt JF. 1998. Circular intermediates of recombinant adeno-associated virus have defined structural characteristics responsible for long-term episomal persistence in muscle tissue. J Virol 72:8568–8577. https://doi.org/10.1128/JVI.72.11.8568-8577.1998.
52. Yang J, Zhou W, Zhang Y, Zidon T, Ritchie T, Engelhardt JF. 1999. Concatamerization of adeno-associated virus circular genomes occurs through intermolecular recombination. J Virol 73:9468–9477. https://doi.org/10.1128/JVI.73.11.9468-9477.1999.
53. Straus SE, Sebring ED, Rose JA. 1976. Concatemers of alternating plus and minus strands are intermediates in adenovirus-associated virus DNA synthesis. Proc Natl Acad Sci U S A 73:742–746. https://doi.org/10.1073/pnas.73.3.742.

54. Cotmore SF, Nüesch JP, Tattersall P. 1993. Asymmetric resolution of a parvovirus palindrome in vitro. J Virol 67:1579–1589. https://doi.org/10.1128/JVI.67.3.1579-1589.1993.
55. Cotmore SF, Nuesch JP, Tattersall P. 1992. In vitro excision and replication of 5' telomeres of minute virus of mice DNA from cloned palindromic concatemer junctions. Virology 190:365–377. https://doi.org/10.1016/0042-6822(92)91223-h.
56. Cotmore SF, Tattersall P. 1988. The NS-1 polypeptide of minute virus of mice is covalently attached to the 5' termini of duplex replicative-form DNA and progeny single strands. J Virol 62:851–860. https://doi.org/10.1128/JVI.62.3.851-860.1988.
57. Cotmore SF, Christensen J, Nüesch JP, Tattersall P. 1995. The NS1 polypeptide of the murine parvovirus minute virus of mice binds to DNA sequences containing the motif [ACCA]2–3. J Virol 69:1652–1660. https://doi.org/10.1128/JVI.69.3.1652-1660.1995.
58. Dettwiler S, Rommelaere J, Nüesch JP. 1999. DNA unwinding functions of minute virus of mice NS1 protein are modulated specifically by the lambda isoform of protein kinase C. J Virol 73:7410–7420. https://doi.org/10.1128/JVI.73.9.7410-7420.1999.
59. Buis J, Wu Y, Deng Y, Leddon J, Westfield G, Eckersdorff M, Sekiguchi JM, Chang S, Ferguson DO. 2008. Mre11 nuclease activity has essential roles in DNA repair and genomic stability distinct from ATM activation. Cell 135:85–96. https://doi.org/10.1016/j.cell.2008.08.015.
60. Williams RS, Moncalian G, Williams JS, Yamada Y, Limbo O, Shin DS, Groocock LM, Cahill D, Hitomi C, Guenther G, Moiani D, Carney JP, Russell P, Tainer JA. 2008. Mre11 dimers coordinate DNA end bridging and nuclease processing in double-strand-break repair. Cell 135:97–109. https://doi.org/10.1016/j.cell.2008.08.017.
61. Salifou K, Burnard C, Basavarajaiah P, Grasso G, Helsmoortel M, Mac V, Depierre D, Franckhauser C, Beyne E, Contreras X, Dejardin J, Rouquier S, Cuvier O, Kiernan R. 2021. Chromatin-associated MRN complex protects highly transcribing genes from genomic instability. Sci Adv 7:eabb2947. https://doi.org/10.1126/sciadv.abb2947.
62. Porro A, Feuerhahn S, Lingner J. 2014. TERRA-reinforced association of LSD1 with MRE11 promotes processing of uncapped telomeres. Cell Rep 6:765–776. https://doi.org/10.1016/j.celrep.2014.01.022.
63. Li S, Lavagnino Z, Lemacon D, Kong L, Ustione A, Ng X, Zhang Y, Wang Y, Zheng B, Piwnica-Worms H, Vindigni A, Piston DW, You Z. 2019. Ca2+-stimulated AMPK-dependent phosphorylation of exo1 protects stressed replication forks from aberrant resection. Mol Cell 74:1123–1137.e6. https://doi.org/10.1016/j.molcel.2019.04.003.
64. Menolfi D, Zha S. 2020. ATM, ATR and DNA-PKcs kinases—the lessons from the mouse models: inhibition ≠ deletion. Cell Biosci 10:8. https://doi.org/10.1186/s13578-020-0376-x.
65. Yin B, Lee BS, Yang-Iott KS, Sleckman BP, Bassing CH. 2012. Redundant and nonredundant functions of ATM and H2AX in $\alpha\beta$ T-lineage lymphocytes. J Immunol 189:1372–1379. https://doi.org/10.4049/jimmunol.1200829.
66. Sakakibara N, Chen D, Jang MK, Kang DW, Luecke HF, Wu SY, Chiang CM, McBride AA. 2013. Brd4 is displaced from HPV replication factories as they expand and amplify viral DNA. PLoS Pathog 9:e1003777. https://doi.org/10.1371/journal.ppat.1003777.